A column of grains in the jamming limit: glassy dynamics in the compaction process

J.M. Luck, A. Mehta

A column of grains in the jamming limit: glassy dynamics in the compaction process

J.M. Luck[a,1] and Anita Mehta[b,2]

[a]Service de Physique Théorique[3], CEA Saclay, 91191 Gif-sur-Yvette cedex, France
[b]S.N. Bose National Centre for Basic Sciences, Block JD, Sector 3, Salt Lake, Calcutta 700098, India

Abstract

We investigate a stochastic model describing a column of grains in the jamming limit, in the presence of a low vibrational intensity. The key control parameter of the model is the reduced void space ε. Regularity and irregularity in grain shapes, respectively corresponding to rational and irrational values of ε, are shown to be centrally important in determining the statics and dynamics of the compaction process.

To be submitted for publication to the European Physical Journal B
P.A.C.S.: 45.70.–n, 45.70.Cc, 45.70.Mg

[1]luck@spht.saclay.cea.fr
[2]anita@boson.bose.res.in
[3]URA 2306 of CNRS

1 Introduction

The study of slow dynamics in the jamming limit unifies the fields of granular compaction [1, 2] and glasses [3]. Key features of this involve frustration and hysteresis, among other complex phenomena, with the concomitant difficulty of modelling them in simple and physical ways. We present in the following a model of remarkable simplicity, which is nevertheless able to capture to a large extent the complex consequences of non-trivial interactions *even in one dimension*. Issues that are probed include the effects of orientation, and thus shape on packing in the jamming limit. 'Irregular' and 'regular' shapes of units (for example, grains) in ways that are shortly to be defined are seen to have rather different consequences for compaction behaviour, when they are subjected to zero- and low-temperature dynamics. The present model has already been introduced in [4] and some of its static and dynamical features have been described in [5]. Here, we give a complete and detailed account of our exploration of this model so far.

2 The model

Our model for grain compaction in the glassy regime is defined as follows [4, 5]. We consider a column of N sites, each of which is occupied by a grain. Grains have an anisotropic shape, so that their orientation matters. For simplicity, we assume that grains can only have two different orientations, referred to as 'ordered' and 'disordered'. The orientation of grain n is translated into a binary variable or 'spin' $\sigma_n = \pm$, with $\sigma_n = +$ denoting an ordered grain, and $\sigma_n = -$ denoting a disordered grain. While ordered grains are perfectly packed, disordered grains are imperfectly packed. Each disordered grain leaves a *void space* ε on the site it inhabits. A configuration of the system is uniquely defined by the orientation variables $\{\sigma_n\}$. Non-trivial dynamical interactions between the grains are such as to minimise the void space *locally*. These can be thought of in terms of an ordering field [5] h_n which reads

$$h_n = \varepsilon\, m_n^- - m_n^+, \tag{2.1}$$

where m_n^+ and m_n^- are respectively the numbers of ordered $(+)$ and disordered $(-)$ grains above grain n:

$$m_n^+ = \frac{1}{2}\sum_{k=1}^{n-1}(1+\sigma_k), \qquad m_n^- = \frac{1}{2}\sum_{k=1}^{n-1}(1-\sigma_k). \tag{2.2}$$

From this we see that h_n is nothing but the *excess void space* [6] of the system. Equation (2.1) shows that a transition from an ordered to a disordered state for grain n is therefore *hindered* by the number of voids that are already above it. A rich ground-state structure is achieved for $\varepsilon > 0$, because of *frustration* [7], whose nature depends on whether ε is rational or irrational. We mention for completeness that the case $\varepsilon < 0$ is a generalisation of earlier work [8], with a complete absence of frustration and a single ground state of ordered grains.

Let us now give a rather more general derivation of the simple physical picture above. In the presence of a dimensionless vibration intensity Γ, we consider a stochastic dynamics, defined by the orientation-flipping rates

$$\begin{cases} w_n(+ \to -) = \exp\left(-\dfrac{\lambda_n + h_n}{\Gamma}\right), \\ w_n(- \to +) = \exp\left(-\dfrac{\lambda_n - h_n}{\Gamma}\right). \end{cases} \tag{2.3}$$

In these expressions, h_n and $\lambda_n \geq 0$ are, respectively, the local ordering field and the activation energy felt by grain number n.

We assume that these quantities only depend on the orientations of grains *above* grain n. For simplicity, we postulate the linear formulas

$$h_n = A\, m_n^+ + B\, m_n^-, \qquad \lambda_n = C\, m_n^+ + D\, m_n^-, \tag{2.4}$$

where $m_n^\pm$ have been defined in (2.2), so that $m_n^+ + m_n^- = n$, while A, B, C, and D are phenomenological parameters.

Hereafter we will focus on the minimal model incorporating the concept of void space introduced above [4, 5]. With an appropriate choice of units, we have

$$A = -1, \qquad B = \varepsilon > 0, \tag{2.5}$$

so that (2.1) is recovered as

$$h_n = \varepsilon\, m_n^- - m_n^+ = \sum_{k=1}^{n-1} \left(\frac{\varepsilon - 1}{2} - \frac{\varepsilon + 1}{2}\,\sigma_k\right), \tag{2.6}$$

Furthermore we assume that the activation energy λ_n does not depend on grain orientations. We define the dynamical length ξ_{dyn} by setting

$$C = D = \frac{\Gamma}{\xi_{\mathrm{dyn}}}, \tag{2.7}$$

so that

$$\lambda_n = \frac{n\Gamma}{\xi_{\mathrm{dyn}}}. \tag{2.8}$$

In order to perform numerical Monte-Carlo simulations we will need a discrete-time formulation of the above rules. The flipping rates w_n become flipping probabilities

$$\begin{cases} p_n(+ \to -) = \dfrac{P_n}{1 + \exp(2h_n/\Gamma)}, \\ p_n(- \to +) = \dfrac{P_n}{1 + \exp(-2h_n/\Gamma)}, \end{cases} \tag{2.9}$$

where the factor

$$P_n = \exp\left(-\frac{\lambda_n}{\Gamma}\right) = \exp\left(-\frac{n}{\xi_{\mathrm{dyn}}}\right) \tag{2.10}$$

describes the *a priori* exponential slowing down of the dynamics with depth n.

In the glassy regime where there are no holes, our earlier model [8, 4] is defined by the rates

$$\begin{cases} w_n(+\to -) = \exp\left(-\dfrac{\Delta h + \Delta H}{\Gamma}\, n\right), \\ w_n(-\to +) = \exp\left(-\dfrac{\Delta h}{\Gamma}\, n\right). \end{cases} \tag{2.11}$$

These rates are recovered by setting

$$A = B = \frac{\Delta H}{2}, \qquad C = D = \frac{\Delta H}{2} + \Delta h. \tag{2.12}$$

The quantities ΔH and Δh are given in simple geometrical terms for hard rectangular grains of sides 1 and $a \leq 1$, i.e., $\Delta H = (1-a)/2$, $\Delta h = (\sqrt{1+a^2}-1)/2$. More generally, ΔH and Δh can be viewed as phenomenological parameters, defining the two characteristic lengths of the model, the equilibrium length $\xi_{\rm eq}$ and the dynamical length $\xi_{\rm dyn}$, which read [8, 4]

$$\xi_{\rm eq} = \frac{\Gamma}{\Delta H}, \qquad \xi_{\rm dyn} = \frac{\Gamma}{\Delta h}. \tag{2.13}$$

We emphasise that in the fully general situation where there are no restrictions on parameter values, the rates (2.3) depend only on the orientations of grains above the grain under consideration. Our new model is therefore a fully directed model of interacting grains, where causality induces a *directionality* both in time and in space, as the orientation of a given grain only influences the grains *below* it, and at *later* times.

3 Zero-temperature statics

As the dynamical rules (2.3) are fully directional, they clearly cannot obey detailed balance. Our discussion of 'temperature' in such an obviously non-equilibrium situation follows established lines [2, 1] regarding its formulation in gently vibrated granular media. In the case of the present model, the determination of the steady state(s) of the system is a non-trivial task.

The dynamics simplifies in the $\Gamma \to 0$ limit [4]. Equation (2.3) indeed yields

$$\frac{w_n(-\to +)}{w_n(+\to -)} = \exp\left(\frac{2h_n}{\Gamma}\right) \to \begin{cases} \infty & \text{if} \quad h_n > 0, \\ 0 & \text{if} \quad h_n < 0. \end{cases} \tag{3.1}$$

From a purely *static* viewpoint, *ground states* of the system can therefore be defined by the condition that the orientation of every grain is aligned along its local field, according to the deterministic equation:

$$\sigma_n = \operatorname{sign} h_n = \begin{cases} + & \text{if} \quad h_n > 0, \\ - & \text{if} \quad h_n < 0, \end{cases} \tag{3.2}$$

provided $h_n \neq 0$ (see below). The condition (3.2) only involves the parameter ε [see (2.1), (2.6)]. It is recursive, because of directionality in that the right-hand side at depth n only involves upper grains $k = 1, \ldots, n-1$. The uppermost orientation σ_1 is left unspecified, as the corresponding local field vanishes identically: $h_1 = 0$. In the following, we assume for definiteness that the uppermost grain is ordered:

$$\sigma_1 = +. \tag{3.3}$$

It turns out that the zero-temperature rule (3.2) yields a rich ground-state structure, because of subtle commensurability and frustration effects. Our starting point is to observe that (3.2) implies

$$\begin{cases} h_n > 0 \Longrightarrow \sigma_n = +, & m^+_{n+1} = m^+_n + 1, & m^-_{n+1} = m^-_n, & h_{n+1} = h_n - 1, \\ h_n < 0 \Longrightarrow \sigma_n = -, & m^+_{n+1} = m^+_n, & m^-_{n+1} = m^-_n + 1, & h_{n+1} = h_n + \varepsilon. \end{cases} \tag{3.4}$$

Surprisingly enough, the number and the nature of ground states depend on the number-theoretic nature of ε. Rational and irrational values of ε will be considered separately.

3.1 Irrational ε: unique quasiperiodic ground state

For irrational ε, (3.4) implies recursively that all the local fields h_n are non-zero, and that they lie in the bounded interval

$$-1 \leq h_n \leq \varepsilon. \tag{3.5}$$

Let us introduce the following *superspace formalism*. Consider the integers (m^-_n, m^+_n) as the co-ordinates of points on a square lattice. We thus obtain a broken, staircase-shaped line, starting as $(m^-_1, m^+_1) = (0,0)$, $(m^-_2, m^+_2) = (0,1)$ [see (3.3)], etc. Vertical steps correspond to ordered $(+)$ grains, whereas horizontal steps correspond to disordered $(-)$ grains, Equation (3.5) defines an oblique strip with *slope* ε in the (m^-, m^+) plane, which contains the entire broken line thus constructed (see Figure 1).

A unique infinite configuration of grain orientations (i.e., a unique broken line) is thus generated. This configuration is *quasiperiodic*. Indeed the above construction is nothing but the cut-and-project method of generating quasiperiodic tilings of the line, which has been extensively studied [9] in the framework of quasicrystals. (Had we made the initial choice $\sigma_1 = -$ instead of (3.3), we would have obtained the same quasiperiodic configuration, up to a permutation of the two uppermost grains.) We mention for further reference the following explicit expressions[1] for $m^\pm_n$ and h_n:

$$m^+_n = n - m^-_n = 1 + \mathrm{Int}((n-1)\Omega), \qquad h_n = -1 + \frac{\mathrm{Frac}((n-1)\Omega)}{1-\Omega}, \tag{3.6}$$

where the rotation number Ω reads

$$\Omega = \frac{\varepsilon}{1+\varepsilon} \qquad (0 < \Omega < 1). \tag{3.7}$$

[1] $\mathrm{Int}(x)$, the integer part of a real number x, is the largest integer less than or equal to x, and $\mathrm{Frac}(x) = x - \mathrm{Int}(x)$ is the fractional part of x $(0 \leq \mathrm{Frac}(x) < 1)$.

An immediate consequence of (3.6) is that there are well-defined proportions of ordered and disordered grains in the ground state:

$$f_+ = \Omega = \frac{\varepsilon}{1+\varepsilon}, \qquad f_- = 1 - \Omega = \frac{1}{1+\varepsilon}. \tag{3.8}$$

This geometrical construction is illustrated in Figure 1 for the most celebrated irrational number, the inverse golden mean [10]:

$$\varepsilon = \Phi - 1 = \frac{1}{\Phi}, \qquad \Omega = 2 - \Phi = \frac{1}{\Phi^2}, \qquad \Phi = \frac{\sqrt{5}+1}{2} \approx 1.618033. \tag{3.9}$$

The corresponding grain configuration is given by a Fibonacci sequence [9, 10]:

$$\{\sigma_n\} = + - - + - - + - + - - + - - + - + - - + - + - - \cdots \tag{3.10}$$

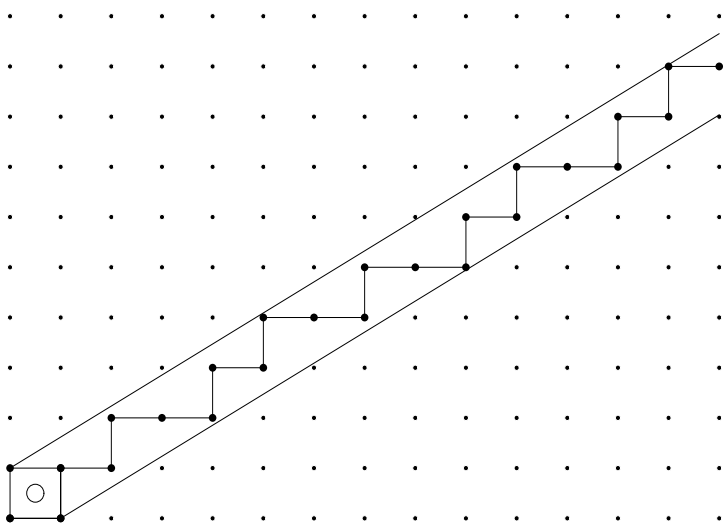

Figure 1: Geometrical construction of the quasiperiodic ground state of the model for the golden-mean slope (3.9). The two ways of going around the first cell, marked with a circle, correspond to the two possible choices for the orientation of the uppermost grain.

3.2 Rational ε: degenerate ground states

For a rational ε:

$$\varepsilon = \frac{p}{q}, \qquad \Omega = \frac{p}{p+q}, \tag{3.11}$$

in irreducible form (p and q are mutual primes), some of the local fields h_n generated by the recursion equations (3.4) vanish. The corresponding grain orientations σ_n remain unspecified. This means that grain n has a perfectly packed column above it, so that it is free to choose its orientation. For $\varepsilon = 1/2$, for example, one can visualise that each disordered grain 'carries' a void half its size, so that units of perfect packing must be

permutations of the triad $+--$, where the two 'half' voids from each of the $-$ grains are filled by the $+$ grain. The dynamics, which is *stepwise compacting*, selects only two of these patterns, $+--$ and $-+-$. More generally, orientational indeterminacy occurs at points of perfect packing such that n is a multiple of the *period* $p+q$.

This feature of rational slopes is clearly visible on the geometrical construction. Figure 2, corresponding to $\varepsilon = 2/3$, shows that some of the lattice cells, marked with circles, are entirely contained in the closed strip (3.5). Consider one such cell. The broken line enters the cell at its lower left corner and exits the cell at its upper right corner. It can go either counterclockwise, via the lower right corner, giving $\sigma_{n+1} = -$, $\sigma_{n+2} = +$, or clockwise, via the upper left corner, giving $\sigma_{n+1} = +$, $\sigma_{n+2} = -$. Each marked cell thus generates a binary choice in the construction. This occurs whenever n is a multiple of the *period* $p+q$, equal to the denominator of the rotation number Ω.

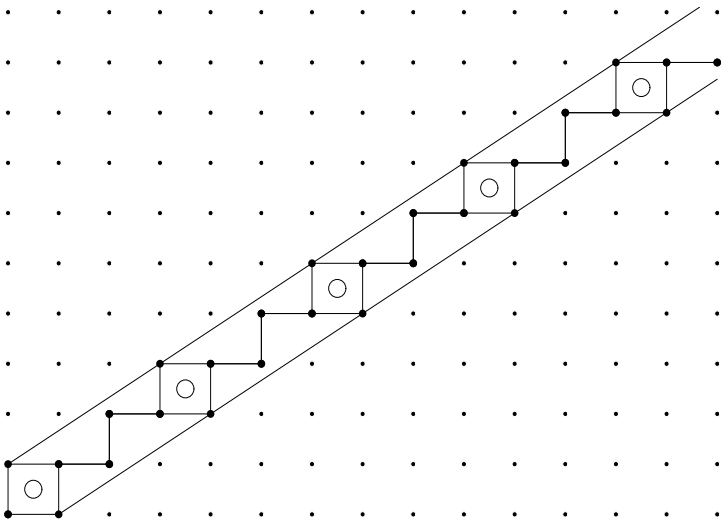

Figure 2: Geometrical construction of the ground states of the model for the rational slope $\varepsilon = 2/3$. The marked cells, entirely contained in the strip, are responsible for the non-zero configurational entropy.

The model therefore has a non-zero ground-state entropy, or zero-temperature configurational entropy,

$$\Sigma = \frac{\ln 2}{p+q} \tag{3.12}$$

per grain. Each ground state is a binary random sequence of two well-defined patterns of length $p+q$, each of them made of p ordered and q disordered ones, so that (3.8) holds for each of the ground states. The patterns only differ by their first two orientations. The simplest cases are listed in Table 1.

The period $p+q$ is formally infinite for an irrational slope. Accordingly, there is only one marked cell in Figure 1, for $n = 0$, corresponding to the fact that only the uppermost grain is unspecified.

period $p+q$	rot. number Ω	slope ε	p	q	pattern 1	pattern 2
2	1/2	1	1	1	$+-$	$-+$
3	1/3	1/2	1	2	$+--$	$-+-$
3	2/3	2	2	1	$+-+$	$-++$
4	1/4	1/3	1	3	$+---$	$-+--$
4	3/4	3	3	1	$+-++$	$-+++$
5	1/5	1/4	1	4	$+----$	$-+---$
5	2/5	2/3	2	3	$+--+-$	$-+-+-$
5	3/5	3/2	3	2	$+-+-+$	$-++-+$
5	4/5	4	4	1	$+-+++$	$-++++$
6	1/6	1/5	1	5	$+-----$	$-+----$
6	5/6	5	5	1	$+-+++++$	$-++++++$

Table 1: Patterns building up the random ground states for the first rational values of ε. The second example with period 5 is illustrated in Figure 2.

4 Zero-temperature dynamics

We now turn to the investigation of the zero-temperature dynamics of the model, given by the rule

$$\sigma_n \to \operatorname{sign} h_n, \tag{4.1}$$

according to (3.1), with the definition (2.1), (2.6). Irrational and rational values of ε will again be dealt with separately.

4.1 Irrational ε, infinite $\xi_{\rm dyn}$: ballistic coarsening

For irrational ε, the rule (4.1) is always well-defined, as the local fields h_n never vanish. We start with the situation where $\xi_{\rm dyn}$ is infinite. We assume that the system is initially in a disordered state, where each grain is oriented at random: $\sigma_n = \pm$ with equal probabilities, except for the uppermost one, which is fixed according to (3.3).

The zero-temperature dynamics is observed to drive the system to its quasiperiodic ground state. This ordering propagates down the system from its top surface, via *ballistic coarsening*. At time t, the grain orientations have converged to their ground-state values, given by the above geometrical construction, in an upper layer whose depth is observed to grow linearly with time:

$$L(t) \approx Vt, \tag{4.2}$$

whereas the rest of the system is still nearly in its disordered initial state.

This phenomenon is similar to phase ordering, as order propagates over a macroscopic length $L(t)$ which grows forever. It is however different from usual coarsening, as the depth of the ordered region grows ballistically, vith a well-defined ε-dependent ordering velocity V, instead of diffusively, or even more slowly [11]. The ordering velocity obeys

the symmetry property $V(\varepsilon) = V(1/\varepsilon)$. Figure 3 shows a plot of the inverse of the ordering velocity, measured in a numerical simulation, against ε, for $0 < \varepsilon < 1$. This velocity is observed to vary smoothly with ε, although it is only defined for irrational ε, and to diverge as $V \sim 1/\varepsilon$ as $\varepsilon \to 0$.

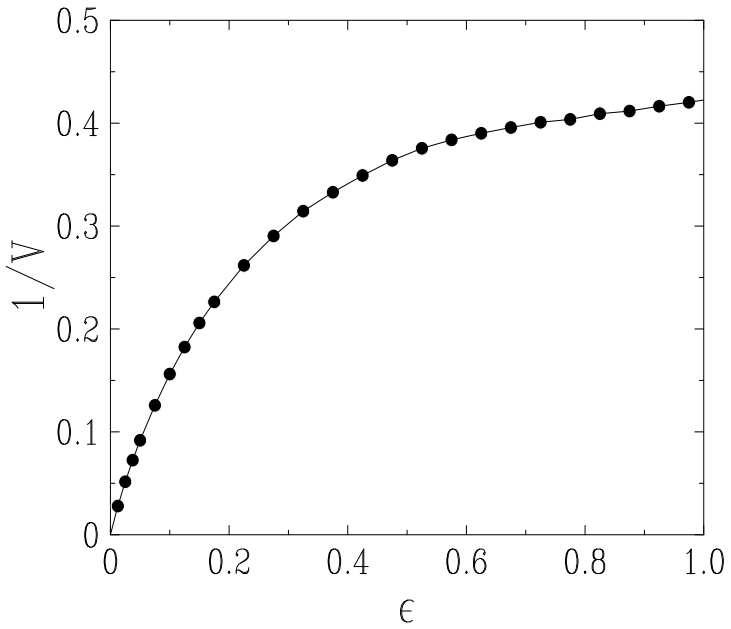

Figure 3: Plot of the inverse ordering velocity $1/V$ of zero-temperature coarsening dynamics at infinite $\xi_{\rm dyn}$, against the irrational slope ε, for $0 < \varepsilon < 1$.

4.2 Irrational ε, finite $\xi_{\rm dyn}$: crossover to logarithmic coarsening

For irrational ε, in the situation where $\xi_{\rm dyn}$ is finite, but large at the microscopic scale of a grain, the ballistic coarsening law (4.2) is modified in order to take the slowing down factor (2.10) into account:

$$\frac{{\rm d}L}{{\rm d}t} \approx V \, \exp\left(-\frac{L}{\xi_{\rm dyn}}\right), \tag{4.3}$$

hence

$$L(t) \approx \xi_{\rm dyn} \ln\left(1 + \frac{Vt}{\xi_{\rm dyn}}\right). \tag{4.4}$$

Equation (4.4) exhibits a crossover between the ballistic law (4.2) for $1 \ll Vt \ll \xi_{\rm dyn}$, and the logarithmic coarsening law

$$L(t) \approx \xi_{\rm dyn} \ln t, \tag{4.5}$$

already present in the model of non-interacting grains [8, 4], in the opposite regime ($Vt \gg \xi_{\rm dyn} \gg 1$).

The dynamical length $\xi_{\rm dyn}$ thus controls the spatial dependence of dynamical behaviour. In earlier work [8] it was shown to determine the extent to which order propagates down the column, in the glassy regime. This interpretation in terms of an *ordered boundary layer* continues to be valid in the present case: For an initially disordered state, the application of zero-temperature dynamics causes the quasiperiodic ground state to be recovered downwards from the free surface to a depth which grows ballistically with time. When $L(t)$ becomes comparable with $\xi_{\rm dyn}$, the effects of the free surface begin to be damped and in particular for $t \gg \xi_{\rm dyn}/V$, one recovers the logarithmic coarsening law $L(t) \approx \xi_{\rm dyn} \ln t$, widely associated with the slow dynamical relaxation of vibrated sand [12].

Equation (4.4) has been checked against the results of accurate numerical simulations, for the golden-mean slope. Figure 4 shows a scaling plot of numerical data for $L(t)$ corresponding to $\xi_{\rm dyn} = 50$ and 100, together with the prediction (4.4), with no adjustable parameter. The ordering velocity $V \approx 2.58$ is taken from the data of Figure 3.

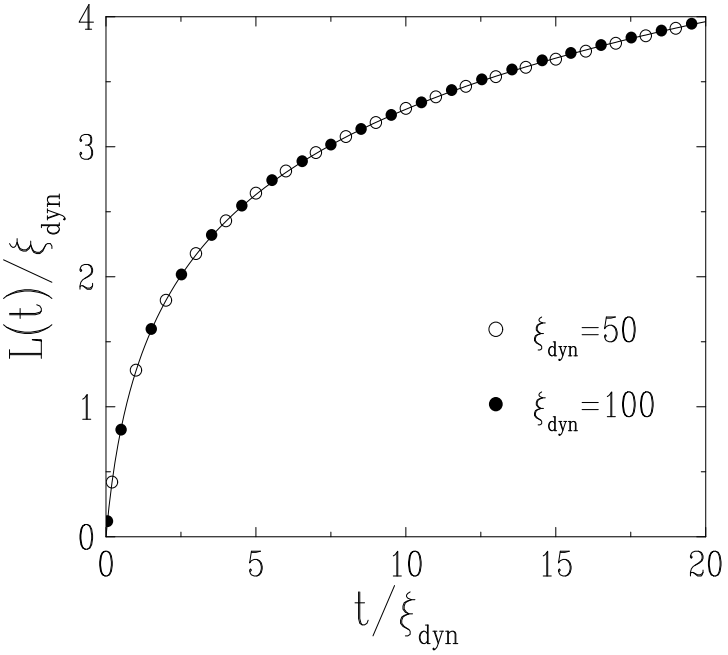

Figure 4: Scaling plot of $L(t)/\xi_{\rm dyn}$ against $t/\xi_{\rm dyn}$ for zero-temperature coarsening dynamics with the golden-mean slope. Symbols: numerical data. Full line: prediction (4.4), with $V = 2.58$.

4.3 Rational ε, infinite $\xi_{\rm dyn}$: anomalous roughening

We now turn to zero-temperature dynamics for rational ε. The updating rule (4.1) is not always well-defined as it stands, as the local fields h_n may now vanish. In such a

circumstance, it is natural to choose the corresponding orientation at random:

$$\sigma_n \to \begin{cases} + & \text{if} \quad h_n > 0, \\ \pm \text{ with prob. } 1/2 & \text{if} \quad h_n = 0, \\ - & \text{if} \quad h_n < 0. \end{cases} \tag{4.6}$$

The zero-temperature dynamics defined in this way therefore keeps a stochastic component. We focus our attention onto the simplest rational case, i.e., $\varepsilon = 1$. Equations (2.1), (2.6) for the local fields read

$$h_n = -\sum_{m=1}^{n-1} \sigma_m. \tag{4.7}$$

We consider first the case where $\xi_{\mathbf{dyn}}$ is infinite. We observe that the zero-temperature dynamics (4.6) does not drive the system to any of its degenerate dimerised ground states. The system rather shows a fast relaxation to a non-trivial steady state, independent of the initial state. We now investigate this novel kind of zero-temperature steady state in some detail, mostly by means of numerical simulations.

Local field fluctuations

First of all, the local fields h_n have unbounded fluctuations in the steady state. Figure 5 shows that these fluctuations have a Gaussian distribution of width W_n, at least deep enough in the system ($n \gg 1$), except for a definite excess of small values of the local field: $|h_n| \sim 1 \ll W_n$. Figure 6 demonstrates that the local field variance grows as

$$W_n^2 = \langle h_n^2 \rangle \approx A\, n^{2/3}, \tag{4.8}$$

with $A \approx 0.83$.

The exponent 2/3 of the *anomalous roughening* law (4.8) can be explained by means of the following local Markovian approximation. Assume that the local field h_n obeys an effective Langevin equation of the form

$$\frac{\mathrm{d}h_n}{\mathrm{d}t} = -a_n h_n + \eta_n(t), \tag{4.9}$$

where $\eta_n(t)$ is a white noise so that $\langle \eta_n(t)\eta_n(t') \rangle = D_n \delta(t-t')$. We then have

$$h_n(t) = h_n(0)\, \mathrm{e}^{-a_n t} + \int_0^t \mathrm{e}^{-a_n(t-t')} \eta_n(t') \mathrm{d}t'. \tag{4.10}$$

In the steady state, h_n is a Gaussian variable of width W_n such that

$$W_n^2 = \langle h_n^2 \rangle = \frac{D_n}{2a_n}. \tag{4.11}$$

The effective parameters a_n and D_n can be estimated as follows. For the deterministic part, (4.6) implies

$$\frac{\mathrm{d}\langle h_n \rangle}{\mathrm{d}t} = \sum_{m=1}^{n-1} \langle \sigma_m - \operatorname{sign} h_m \rangle \approx -(1 - Q_n)\langle h_n \rangle, \tag{4.12}$$

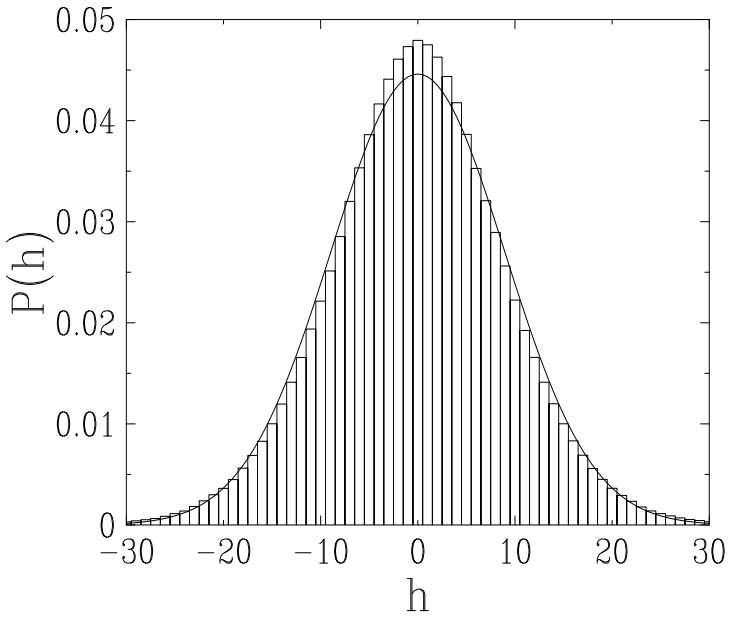

Figure 5: Plot of the distribution of the local field h_n for $n \approx 1000$. Histogram: numerical data (data for $n = 999$ and $n = 1000$ are mixed in order to avoid spurious parity effects). Full curve: Gaussian law with width $W_{1000} = 8.94$.

where the order parameter Q_n is defined as

$$Q_n = \langle \sigma_n \operatorname{sign} h_n \rangle. \tag{4.13}$$

The latter quantity will be shown below to fall off as $n^{-1/3}$ [see (4.25)], implying $a_n \approx 1$. The absence of divergence of the relaxation time $\tau_n = 1/a_n$ with n explains the observed fast relaxation to the steady state. As the fluctuating part is due to the second line of (4.6), the strength of the noise D_n reads, in some units,

$$D_n \approx b \sum_{m=1}^{n-1} \mathrm{Prob}\{h_m = 0\} \approx \frac{b}{\sqrt{2\pi}} \sum_{m=1}^{n-1} \frac{1}{W_m}, \tag{4.14}$$

assuming that the h_n have a Gaussian distribution. Equation (4.11) yields

$$W_n^2 \approx \frac{b}{2\sqrt{2\pi}} \sum_{m=1}^{n-1} \frac{1}{W_m}, \tag{4.15}$$

hence the power law (4.8), with $A = (9b^2/(32\pi))^{1/3}$.

The anomalous roughening law (4.8) is the most central feature of the zero-temperature steady state observed for rational ε. Exponents 1/3 and 2/3 in one-dimensional models may show up in various contexts. In the present situation [5], the mechanism at work is analogous to the domain-growth mechanism in the low-temperature coarsening regime of the Ising chain with Kawasaki dynamics [13]: the power law $L(t) \sim t^{1/3}$ for the mean domain size (analogous to $W_n \sim n^{1/3}$) can be understood from the picture of diffusing domains, whose diffusion constant scales as the inverse of their length.

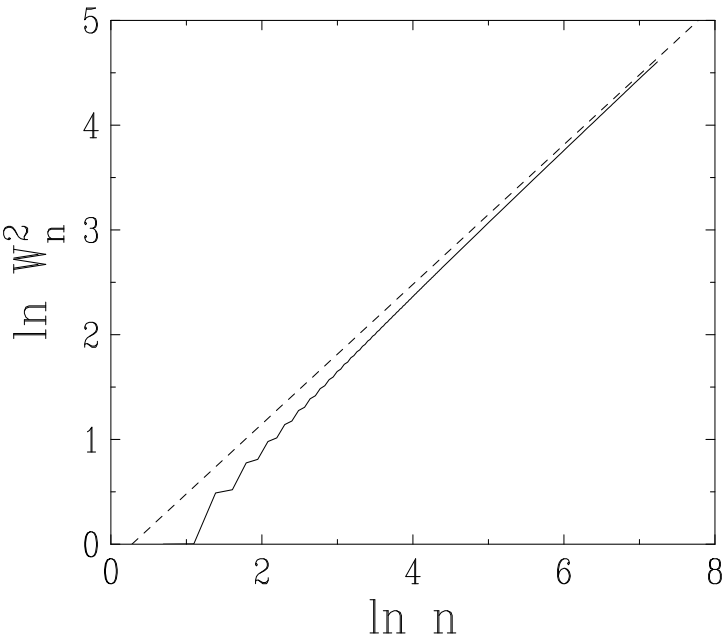

Figure 6: Log-log plot of $W_n^2 = \langle h_n^2 \rangle$ against depth n, for zero-temperature dynamics with $\varepsilon = 1$. Full line: numerical data. Dashed line: fit to asymptotic behaviour, leading to (4.8) (after [5]).

Orientation and local field correlations

If the grain orientations were statistically independent, i.e., uncorrelated, one would have the simple result $\langle h_n^2 \rangle = n\varepsilon$, while (4.8) implies that $\langle h_n^2 \rangle$ grows much more slowly than n. The orientational displacements of each grain are therefore *fully anticorrelated.* We discuss the physical implications of this first, before focusing on details below. The anticorrelated orientational displacements are reminiscent of the *bridge collapse* seen in displacement-displacement correlations of strongly compacting grains [14]; grain orientational displacements in the direction of vibration were there seen to be strongly anticorrelated in jammed regions, as each grain tried to collapse into the void space trapped by its neighbours. We remark that temporal anticorrelations have also been observed in recent experiments investigating the properties of cages near the colloidal glass transition [15]. Interestingly, correlations *transverse* to the shaking direction were [14] found to be rather small, thus, in self-consistency terms justifying the choice of a column model in the present case.

To be more specific, let us denote the orientation and local field correlation functions as

$$c_{m,n} = \langle \sigma_m \sigma_n \rangle, \qquad C_{m,n} = \langle h_m h_n \rangle. \tag{4.16}$$

Equation (4.7) implies

$$C_{m,n} = \sum_{k=1}^{m-1} \sum_{\ell=1}^{n-1} c_{k,\ell}, \qquad c_{m,n} = C_{m+1,n+1} - C_{m+1,n} - C_{m,n+1} + C_{m,n}, \tag{4.17}$$

and especially

$$c_{n,n} = C_{n+1,n+1} - 2C_{n,n+1} + C_{n,n} = 1. \tag{4.18}$$

The latter property implies $C_{n,n} - C_{n,n\pm1} \approx 1/2$, and more generally

$$C_{n,n} - C_{n,n+k} \approx \frac{|k|}{2} \qquad (|k| \ll n). \tag{4.19}$$

This behaviour and the power law (4.8) can be combined into the following scaling Ansatz:

$$C_{m,n} \approx W_m W_n \, \mathcal{F}\Big(\frac{n-m}{W_m W_n}\Big), \tag{4.20}$$

where $\mathcal{F}$ is a positive, even function, with a cusp at the origin of the form

$$\mathcal{F}(x) = 1 - \frac{|x|}{2} + \cdots \qquad (|x| \ll 1). \tag{4.21}$$

As a consequence of (4.17), the orientation correlations obey a similar scaling law:

$$c_{m,n} \approx \delta_{m,n} - \frac{1}{W_m W_n} \, F\Big(\frac{n-m}{W_m W_n}\Big), \tag{4.22}$$

where $F(x) = \mathrm{d}^2\mathcal{F}/\mathrm{d}x^2$ is another positive, even function such that

$$\int_{-\infty}^{+\infty} F(x)\,\mathrm{d}x = \int_0^{+\infty} x\,F(x)\,\mathrm{d}x = 1. \tag{4.23}$$

The first of these sum rules confirms that spin fluctuations are asymptotically *totally screened*: $\sum_{m\neq n} c_{n,n} \approx -c_{n,n} = -1$. The scaling laws (4.20) and (4.22) are accurately confirmed by numerical data for $C_{m,n}$ and $c_{m,n}$, whose scaling plots are respectively shown in Figures 7 and 8.

A final consequence concerns the mixed correlation

$$\langle \sigma_n h_n \rangle = \sum_{m=1}^{n-1} c_{m,n}, \tag{4.24}$$

for which the scaling results (4.20), (4.22) yield $\langle \sigma_n h_n \rangle \approx 1/2$. Scaling then implies that the order parameter defined in (4.13) behaves as $Q_n \sim 1/W_n$, hence the estimate

$$Q_n \approx a\, n^{-1/3}. \tag{4.25}$$

This power-law fall off is well confirmed by numerical data, shown in Figure 9, which yield $a \approx 0.44$.

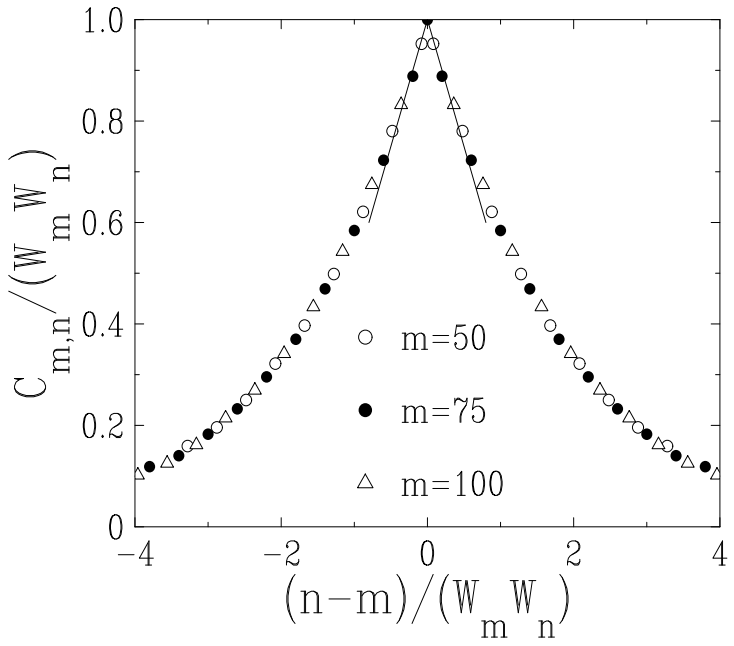

Figure 7: Scaling plot of the correlation function $C_{m,n}$ of the local fields in the zero-temperature steady state with $\varepsilon = 1$, demonstrating the validity of (4.20), and showing a plot of the scaling function $\mathcal{F}$. The full lines show the cusp behaviour (4.21).

Entropy

We now turn to the evaluation of the dimensionless entropy of the steady state, defined by the usual Boltzmann formula

$$S = -\sum_{\mathcal{C}} p(\mathcal{C}) \ln p(\mathcal{C}), \tag{4.26}$$

where $p(\mathcal{C})$ is the probability that the system is in the orientation configuration $\mathcal{C}$ in the steady state, and the sum runs over all the 2^n configurations $\mathcal{C} = \{\sigma_m\}$ $(m = 1, \ldots, n)$ of a system of n grains.

On the theoretical side, the entropy S can be estimated as follows, using the main feature of the zero-temperature steady state, i.e., the roughening law (4.8). Think of the depth n as a fictitious discrete time, and of the local field h_n as the position of a random walker at time n. For a free lattice random walk of n steps, one has $\langle h_n^2 \rangle = n$, and the entropy reads $S_{\text{flat}} = n \ln 2$, as all configurations are equally probable. Because $\langle h_n^2 \rangle = W_n^2 \ll n$, the entropy S of our random walk is reduced with respect to S_{flat}. Let

$$\Delta S = S_{\text{flat}} - S = n \ln 2 - S \tag{4.27}$$

be the entropy reduction [16]. Consider first a strict constraint $|h_n| < L$. The probability that a random walk of n steps obeys this constraint is known to fall off exponentially, as $\mathcal{P}_n \approx \exp(-\pi^2 n/(2L^2))$. For a slowly time-dependent constraint $|h_n| < L_n$, this estimate

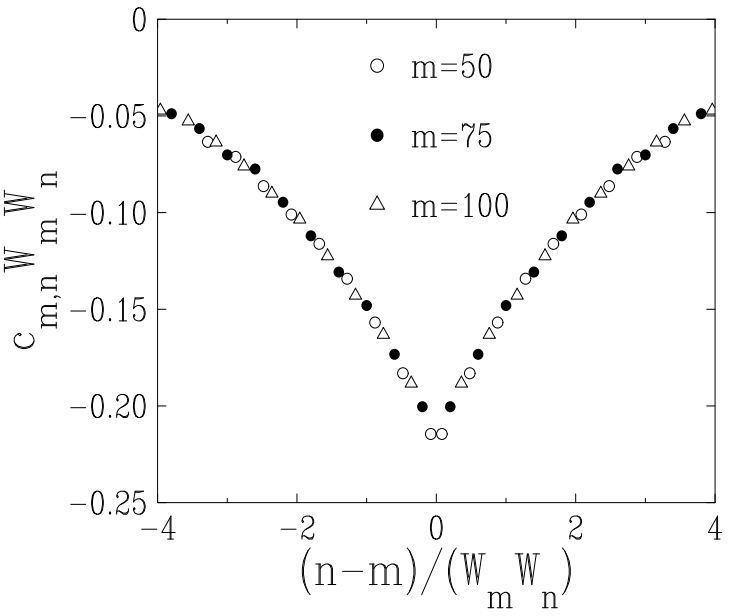

Figure 8: Scaling plot of the orientation correlation function $c_{m,n}$ for $n \neq m$ in the zero-temperature steady state with $\varepsilon = 1$, demonstrating the validity of (4.22), and showing a plot of (minus) the scaling function F (after [5]).

generalises to

$$\mathcal{P}_n \approx \exp\left(-\frac{\pi^2}{2}\sum_{m=1}^{n}\frac{1}{L_m^2}\right). \tag{4.28}$$

With the assumption that the strict constraint $|h_n| < W_n$ and the weak constraint $\langle h_n^2\rangle = W_n$ generate similar entropy reductions for similar constraint profiles, we obtain the estimate

$$\Delta S = -\ln \mathcal{P}_n \sim \sum_{m=1}^{n}\frac{1}{W_m^2} \sim n^{1/3}. \tag{4.29}$$

We have evaluated the steady-state entropy S in a numerical simulation, using its definition (4.26), by measuring the probabilities $p(\mathcal{C})$ of all the configurations. As there are 2^n configurations for a system of n grains, the a priori statistical error only decays as $(2^n/t)^{1/2}$. Reliable data are obtained in this way for $t \sim 10^9$ and $n \approx 20$. Figure 10 shows a plot of the entropy reduction ΔS against n. The data show that ΔS is small, at least for system sizes reachable by numerical simulations. For $n = 12$ (data of Figure 11) we have $\Delta S \approx 0.479$. A reasonable agreement with the estimate (4.29) is found. The fit shown in the plot suggests that (4.29) is affected by a logarithmic correction, which cannot be explained by the simple argument leading to (4.29), with a small amplitude ≈ 0.06.

Figure 11 shows the normalised probabilities $2^n\, p(\mathcal{C})$, for $n = 12$, plotted against the $2^{12} = 4096$ configurations $\mathcal{C}$, sorted according to lexicographical order (i.e., read down the column). This plot exhibits a startlingly rugged structure on this microscopic scale: some configurations are clearly visited far more often than others. We suggest that this

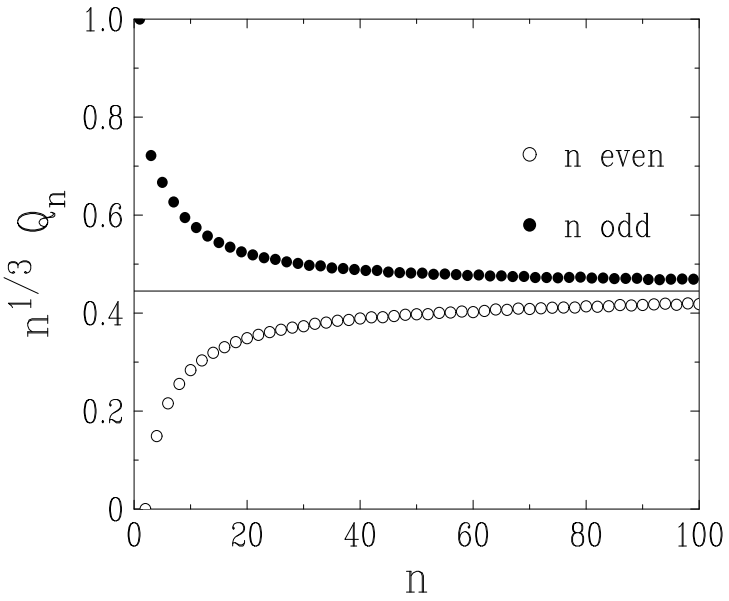

Figure 9: Plot of $n^{1/3}$ times the order parameter Q_n against n, for the zero-temperature steady state with $\varepsilon = 1$, Symbols: numerical data. Full line: common limit value, yielding $a \approx 0.44$ in (4.25).

behaviour is generic: i.e., *the dynamics of compaction in the jammed state leads to a microscopic sampling of configuration space which is highly non-uniform.* In spite of this fine structure, the entropy reduction $\Delta S \sim n^{1/3}$ is negligible with respect to the free entropy $S_{\mathrm{flat}} = n \ln 2$, in qualitative agreement with Edwards' flatness hypothesis [1, 17].

4.4 Rational ε, finite ξ_{dyn}: crossover to Brownian roughening

In the case where ξ_{dyn} is finite, the system still relaxes to a non-trivial steady state, which is qualitatively similar to that obtained for $\xi_{\mathrm{dyn}} = \infty$, investigated above.

At the quantitative level, the main effect of the finiteness of ξ_{dyn} is to induce a nontrivial profile of W_n^2. In the regime where both n and ξ_{dyn} are large, the following scaling law is observed

$$W_n^2 \approx (W_n^2)_\infty \, f\left(\frac{n}{\xi_{\mathrm{dyn}}}\right), \tag{4.30}$$

where $(W_n^2)_\infty$ is given by the anomalous roughening law (4.8) of the $\xi_{\mathrm{dyn}} = \infty$ steady state, which holds more generally for $n \ll \xi_{\mathrm{dyn}}$. One has therefore $f(0) = 1$.

A qualitative understanding of the scaling function f can be obtained by generalising the above Markovian approximation. The expression (4.14) for the strength of the noise is readily replaced by

$$D_n \approx \frac{b}{\sqrt{2\pi}} \sum_{m=1}^{n-1} \frac{\mathrm{e}^{-m/\xi_{\mathrm{dyn}}}}{W_m}. \tag{4.31}$$

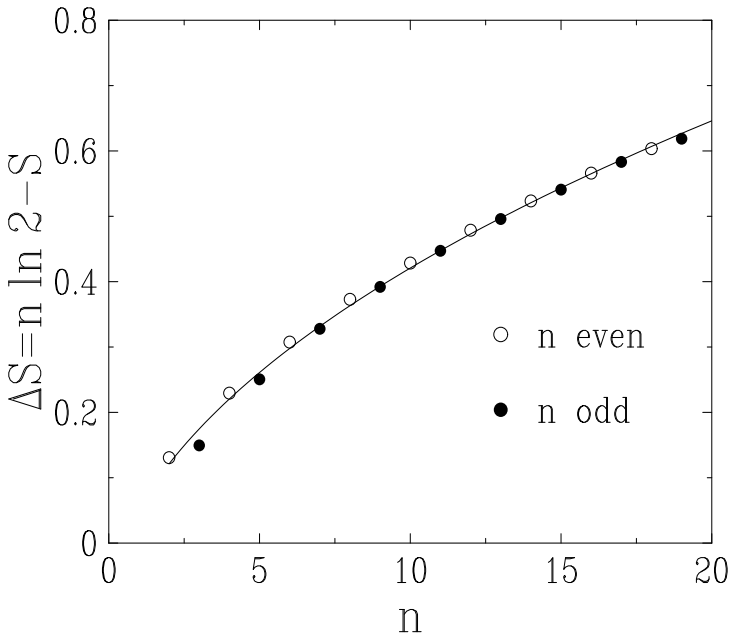

Figure 10: Plot of the measured entropy reduction ΔS in the zero-temperature steady state with $\varepsilon = 1$, defined in (4.27), against $n \leq 19$. Symbols: numerical data. Full line: fit $\Delta S = (62 \ln n + 53) 10^{-3}\, n^{1/3}$.

For the deterministic part, (4.6) implies

$$\frac{\mathrm{d}\langle h_n \rangle}{\mathrm{d}t} = \sum_{m=1}^{n-1} \langle \sigma_m - \operatorname{sign} h_m \rangle \, \mathrm{e}^{-m/\xi_{\mathrm{dyn}}}. \tag{4.32}$$

The right-hand side is not simply related to h_n any more, so that a further level of approximation is needed. The most straightforward choice reads

$$a_n \approx \frac{1}{n} \sum_{m=1}^{n-1} \mathrm{e}^{-m/\xi_{\mathrm{dyn}}} \approx \frac{\xi_{\mathrm{dyn}}}{n} (1 - \mathrm{e}^{-n/\xi_{\mathrm{dyn}}}). \tag{4.33}$$

Skipping the derivation, we mention that (4.31), (4.33) imply (4.30), with

$$f(x) = \frac{x^{1/3}}{1 - \mathrm{e}^{-x}} \left[\int_0^x \left(\frac{1 - \mathrm{e}^{-y}}{y} \right)^{1/2} \mathrm{e}^{-y} \, \mathrm{d}y \right]^{2/3} \approx \begin{cases} 1 + x/12 & (x \ll 1), \\ K\, x^{1/3} & (x \gg 1) \end{cases} \quad (K = 0.87732). \tag{4.34}$$

In view of the crudeness of the above assumptions, (4.34) is only meant to provide a qualitative description of the scaling function f. Its asymptotic behaviour for $x \gg 1$:

$$f(x) \approx K\, x^{1/3}, \qquad W_n^2 \approx \frac{AK\, n}{{\xi_{\mathrm{dyn}}}^{1/3}}, \tag{4.35}$$

is, however, expected to yield the correct dependence on n and ξ_{dyn}. The profile of local fields is thus predicted to be Brownian for $n \gg \xi_{\mathrm{dyn}}$. Figure 12 shows a scaling plot

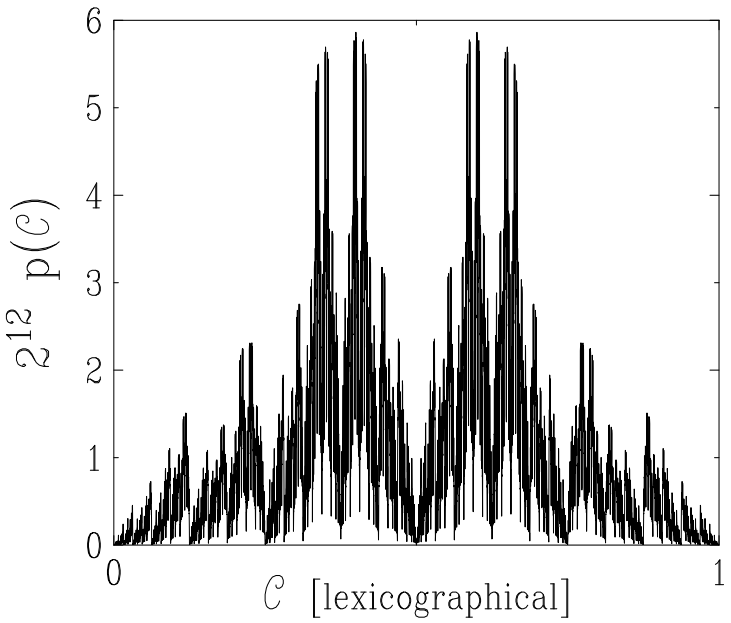

Figure 11: Plot of the normalised probabilities $2^n\, p(\mathcal{C})$ of all the configurations for $n = 12$ in the zero-temperature steady state with $\varepsilon = 1$, against the configuration $\mathcal{C}$ sorted according to lexicographical order (after [5]).

of numerical data for the ratio $W_n^2/(W_n^2)_\infty$, against $x = n/\xi_{\rm dyn}$. A scaling law of the form (4.30) is clearly observed. The fitted curve is compatible with the behaviour (4.35), with $K \approx 2.66$.

5 Low-temperature dynamics

We now turn to the investigation of the low-temperature dynamics of the model. We consider for simplicity the case of an infinite $\xi_{\rm dyn}$. If the slope ε is irrational, the dynamical rule (4.1) is fully deterministic at zero temperature, so that a small non-zero temperature is expected to have drastic effects. To the contrary, for a rational slope ε, the rule (4.6) is already stochastic at zero temperature, and indeed no interesting effect appears at a small non-zero temperature.

We therefore focus our attention onto the case of an irrational slope ε. We recall that the zero-temperature dynamics drives the system to its unique quasiperiodic ground state, where each orientation is aligned with its local field, according to (3.2). For a low but non-zero temperature Γ, there will be *mistakes*, i.e., orientations $\sigma_n = -\operatorname{sign} h_n$ not aligned with their local field. Equation (3.1) suggests that the a priori probability of observing a mistake at site n scales as

$$\Pi(n) \approx \exp\left(-\frac{2|h_n|}{\Gamma}\right). \tag{5.1}$$

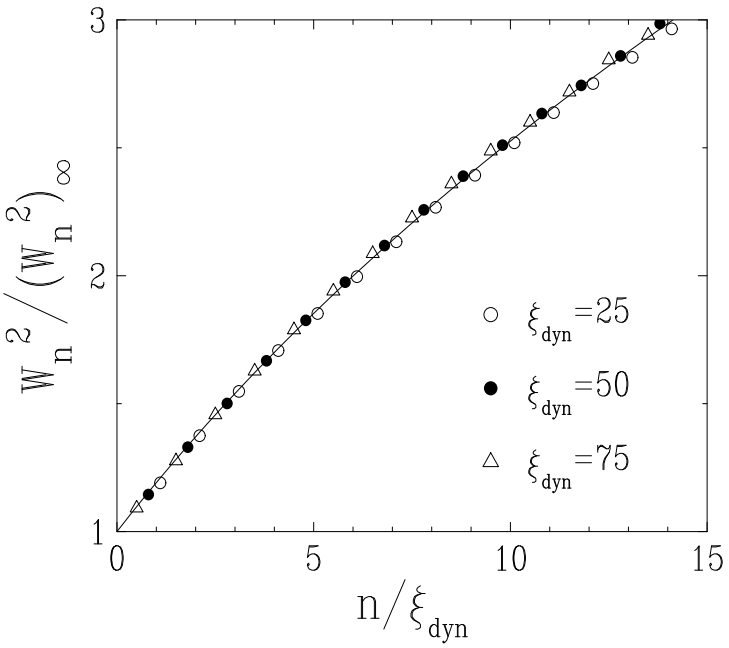

Figure 12: Scaling plot of the ratio $W_n^2/(W_n^2)_\infty$ against $x = n/\xi_{\rm dyn}$ in the zero-temperature steady state with $\varepsilon = 1$, illustrating the scaling law (4.30), and showing a plot of the scaling function f. Symbols: numerical data. Curve: fit $f = 1 + a((1+bx)^{1/3} - 1)$, with $a = 5.63$, $b = 0.105$, so that $K = a\,b^{1/3} = 2.66$.

Hence the sites n such that the local field h_n is relatively small in the ground state ($|h_n| \sim \Gamma \ll 1$) will be nucleation sites for mistakes, and thus govern the low-temperature dynamics, in a sense that will become more precise.

The leading nucleation sites can be located as follows. Equation (3.6) shows that the local field h_n is small when $n\Omega$ is close to an integer m. The latter turns out to be $m = m_n^+$. Indeed

$$n\Omega = m + \delta \Longrightarrow h_n = \frac{\delta}{1-\Omega} \tag{5.2}$$

for δ small enough ($\Omega - 1 < \delta < \Omega$). The leading sites n are thus obtained by finding the rational numbers m/n which are the closest to the rotation number Ω. This is a well-defined problem of Number Theory referred to as Diophantine approximation [10].

5.1 The golden-mean slope

Before we tackle the problem in general, we consider again for definiteness the golden-mean slope (3.9). In this case, we are led to introduce the Fibonacci numbers F_k [9, 10], defined by the recursion formula

$$F_k = F_{k-1} + F_{k-2} \qquad (F_0 = 0, \quad F_1 = 1). \tag{5.3}$$

We have alternatively

$$F_k = \frac{\Phi^k - (-\Phi)^{-k}}{\sqrt{5}}. \tag{5.4}$$

The leading nucleation sites are the Fibonacci sites $n = F_k$. We have $m = m_n^+ = F_{k-2}$, $m_n^- = F_{k-1}$, and

$$h_n = \frac{(-)^k \Phi}{\sqrt{5}\, F_k}, \tag{5.5}$$

so that

$$\Pi_k = \Pi(F_k) \sim \exp\left(-\frac{2\Phi}{\sqrt{5}\,\Gamma F_k}\right). \tag{5.6}$$

We can therefore draw the following picture of low-temperature dynamics. Mistakes are nucleated at Fibonacci sites, according to a Poisson process. They are then advected with constant velocity $V = 2.58$, just as in the zero-temperature case. The system is ordered according to its quasiperiodic ground state in an upper layer ($n < \mathcal{N}(t)$), while the rest is disordered, somehow like the zero-temperature steady state for a rational slope. The depth $\mathcal{N}(t)$ of the ordered layer, given by the position of the *uppermost* mistake, is a collective co-ordinate describing low-temperature dynamics. It evolves according to ballistic advection, i.e., $\mathcal{N}(t_1) = \mathcal{N}(t_0) + V(t_1 - t_0)$, until it jumps backward to a smaller depth $\mathcal{N}(t_1) = F_k$, if another mistake is nucleated there. Figure 13 shows a typical sawtooth plot of the instantaneous depth $\mathcal{N}(t)$, for a temperature $\Gamma = 0.003$. The leading nucleation sites are observed to be given by Fibonacci numbers.

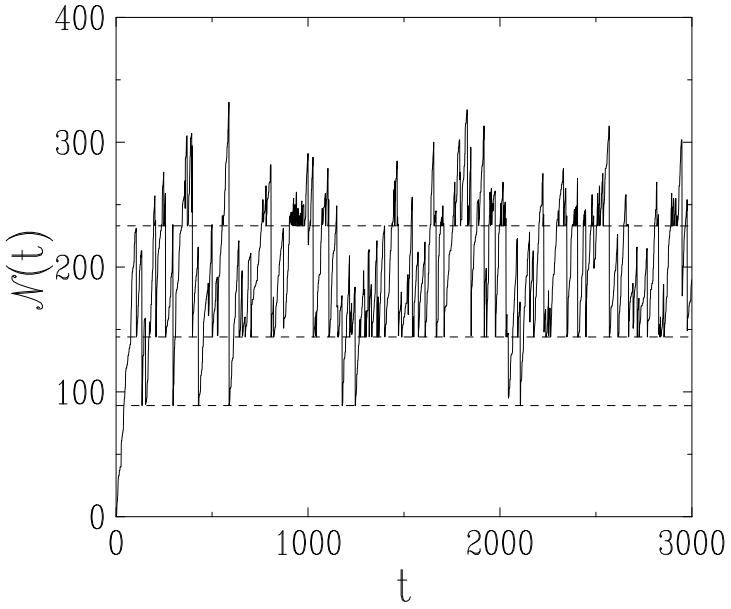

Figure 13: Plot of the instantaneous depth $\mathcal{N}(t)$ of the ordered layer, for the golden-mean slope at $\Gamma = 0.003$. Dashed lines: leading nucleation sites given by consecutive Fibonacci numbers (bottom to top: $F_{11} = 89$, $F_{12} = 144$, $F_{13} = 233$) (after [5]).

The system thus reaches a steady state, characterised by a finite ordering length $\langle \mathcal{N} \rangle$. This length is expected to diverge at low temperature, as mistakes become more and more rare. The law of this divergence can be predicted by the following argument. The most active nucleation Fibonacci site is such that the nucleation time $1/\Pi_k$ is comparable to the advection time to the next nucleation site F_{k+1}, $(F_{k+1} - F_k)/V \approx F_k/(\Phi V)$, hence the estimate

$$\frac{\Pi_k F_k}{\Phi V} \sim 1. \tag{5.7}$$

Indeed, less deep sites have too small nucleation rates, while the mistakes nucleated at deeper sites have little chance to be the uppermost ones. Equations (5.6) and (5.7) yield

$$\frac{\sqrt{5}}{2\Phi} \Gamma F_k \ln \frac{F_k}{\Phi V} \sim 1. \tag{5.8}$$

For $\Gamma = 0.003$, and for the Fibonacci sites shown in Figure 13, the left-hand side of (5.8) respectively reads 0.56 for $F_{11} = 89$, 1.06 for $F_{12} = 144$, and 1.94 for $F_{13} = 233$. The estimate (5.8) therefore correctly predicts the observed fact that $F_{12} = 144$ is the most active nucleation site at that temperature.

The heuristic argument leading to (5.8) can be justified and made more precise by means of the results of Appendix A. The continuum approach is justified because the Fibonacci sites are more and more sparse. In the case of present interest, keeping only the Fibonacci sequence of leading nucleation sites, we obtain the prediction (A.6) for the ordering length $\langle \mathcal{N} \rangle$, shown in Figure 14.

For a low enough temperature Γ, the sum entering the right-hand side of (A.6) is sharply cutoff. It can indeed be shown that the term of order k in that sum is essentially F_{k-1} for $k \leq k^\star$, while it is exponentially negligible for $k \geq k^\star + 1$, where $k^\star = \mathrm{Int}(K)$, and K is the *real* solution of (5.8), considered as a strict equality, with $F_K \approx \Phi^K/\sqrt{5}$, according to (5.4). We have therefore $\langle \mathcal{N} \rangle \approx F_{k^\star+1}$, i.e., more explicitly,

$$\langle \mathcal{N} \rangle \approx F_K \, \mathcal{A}_K. \tag{5.9}$$

The first factor of this expression,

$$F_K \approx \frac{2\Phi}{\sqrt{5}\,\Gamma|\ln\Gamma|} \left(1 - \frac{1}{|\ln\Gamma|} \ln \frac{2\Phi}{V\sqrt{5}\,|\ln\Gamma|} + \cdots \right), \tag{5.10}$$

shows that the ordering length obeys a linear divergence at low temperature, with explicit logarithmic corrections. The second factor,

$$\mathcal{A}_K = \Phi^{1-\mathrm{Frac}(K)}, \tag{5.11}$$

is a periodic function of its argument $K \approx |\ln\Gamma|/\ln\Phi$, with unit period, which oscillates between the bounds $\mathcal{A}_{\max} = \Phi$ and $\mathcal{A}_{\min} = 1$. *Oscillatory amplitudes* are commonly observed in models related to self-similar structures [18]; they originate in the discrete self-similarity of the underlying sequence. The oscillations of the asymptotic amplitude

$\mathcal{A}_K$, given in (5.11), are damped, except at extremely low temperature. Figure 14 shows a plot of numerical data for the product $\Gamma\langle\mathcal{N}\rangle$, against $|\ln\Gamma|$. These data are well described by the analytical prediction (A.6), and lie within the bounds of the asymptotic estimate (5.9)–(5.11). The oscillations become visible on the analytical curve for the lower temperatures ($\Gamma < 10^{-4}$), which are not directly accessible to simulations.

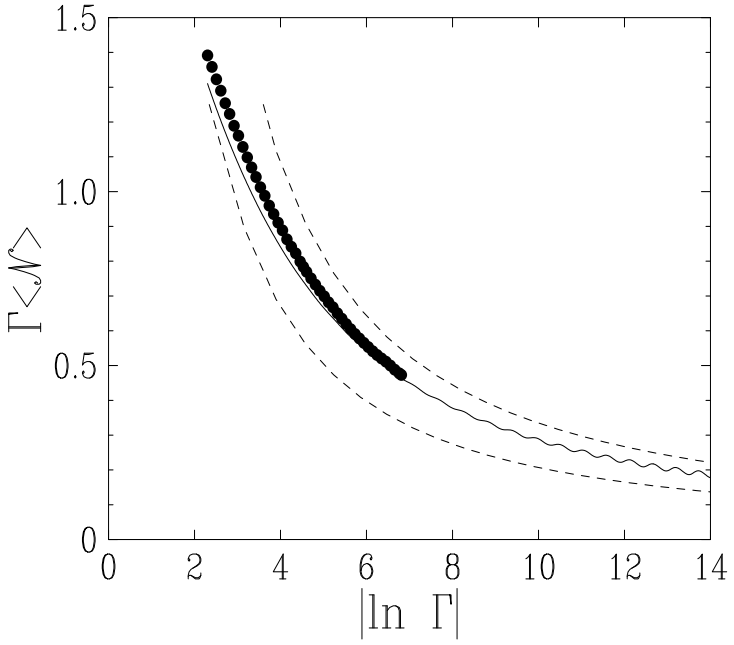

Figure 14: Plot of the product $\Gamma\langle\mathcal{N}\rangle$ against $|\ln\Gamma|$, for the golden-mean slope. Symbols: numerical data. Full line: analytical prediction (A.6). Dashed lines: Extrema of the asymptotic result (5.9), corresponding to $\mathcal{A} = \mathcal{A}_{\max}$ (upper curve) and $\mathcal{A} = \mathcal{A}_{\min}$ (lower curve).

5.2 Other irrational slopes

We now consider briefly the case of an arbitrary irrational slope ε. The situation is rather similar to the phenomenon of hierarchical melting, observed in incommensurate modulated solids [19]. The leading nucleation sites can be determined as follows, along the line of reasoning used to describe hierarchical melting at low temperature.

The irrational rotation number Ω can be written as an infinite *continued-fraction expansion* [10]:

$$\Omega = \cfrac{1}{a_1 + \cfrac{1}{a_2 + \cfrac{1}{a_3 + \cdots}}} = [a_1, a_2, a_3, \ldots]. \tag{5.12}$$

The principal approximants of Ω are the rationals

$$\Omega_k = \frac{p_k}{q_k}, \tag{5.13}$$

whose numerators and denominators obey the same linear recursion

$$p_k = a_k p_{k-1} + p_{k-2}, \qquad q_k = a_k q_{k-1} + q_{k-2}, \tag{5.14}$$

with $p_0 = q_{-1} = 0$, $p_1 = q_0 = 1$. The denominators $n_k = q_k$ define the leading sequence of nucleation sites. The rotation number Ω also has secondary approximants

$$\Omega_{k,b} = \frac{b p_{k-1} + p_{k-2}}{b q_{k-1} + q_{k-2}} \tag{5.15}$$

for $b = 1, \ldots, a_k - 1$ if $a_k > 1$. The denominators $n_{k,b} = b q_{k-1} + q_{k-2}$ define subleading nucleation sites.

For the golden-mean slope, we have $\Omega = 2 - \Phi = [2, 1, 1, 1, 1, \ldots]$, so that the leading Fibonacci nucleation sites of section 5.1 are recovered, whereas there are no subleading nucleation sites.

The most active nucleation site at low temperature can again be estimated by comparing the nucleation time and the advection time. The ordering length $\langle \mathcal{N} \rangle$ is thus still predicted to diverge as

$$\langle \mathcal{N} \rangle \approx \frac{\mathcal{A}(\ln \Gamma)}{\Gamma |\ln \Gamma|}, \tag{5.16}$$

at least for irrational numbers with typical Diophantine properties. Most irrational numbers are typical in this respect. The presence of secondary approximants makes however the oscillation pattern of the amplitude $\mathcal{A}(\ln \Gamma)$ more complex than a simple periodic function in general, in analogy with the low-temperature specific heat peaks induced by the phenomenon of hierarchical melting.

In more physical terms, the ordering length $\langle \mathcal{N} \rangle$ defines the mean position of a fluctuating boundary layer, separating an ordered state above it from a disordered state below. This length is thus a kind of finite-temperature equivalent of the 'zero-temperature' length $\xi_{\rm dyn}$. Both $\langle \mathcal{N} \rangle$ and $\xi_{\rm dyn}$ retain the flavour of a boundary layer separating order from disorder. Within each of these boundary layers, the relaxation is *fast*, and based on single-particle relaxation, i.e., individual particles attaining their positions of optimal local packing [14, 20]. The *slow* dynamics of cooperative relaxation only sets in for lengths *beyond* these, when the lengths over which packing needs to be optimised become non-local. This in turn leads, as in reality [6], to *hysteresis*, i.e., a dependence on the initial state of the packing.

6 Discussion

We have investigated a columnar model describing the effect of grain shape on the statics and dynamics of the compaction process in the glassy regime (long times and weak vibration intensity). One of the main features of the present model is that interactions are fully directional in space and in time: the orientation of a given grain only influences *deeper* grains at *later* times. There is basically one control parameter in the model: the reduced void space ε.

Our main results are as follows. For ε irrational, there is a unique *quasiperiodic* ground state, while when ε is rational, there are a large number of degenerate ground states. Associating (ir)regular grains with (ir)rational void spaces, this has the appealing physical interpretation that irregularities in grain shapes lead to a unique state of close packing (such that all jagged edges are well meshed together), while regular grains have a huge degeneracy of such states (as in the fabled greengrocer's problem [21]). Secondly, zero-temperature dynamics in the irrational case leads to a rather fast retrieval of the quasiperiodic ground state, while in the rational case the ground states are never retrieved, but instead a *non-trivial steady state*, with well-defined density fluctuations [12, 14] about a mean packing fraction, is found. *Local minimisation criteria* thus lead to a *unique, globally optimal configuration* for the irrational case, but not for the rational case, where the frustration present in our model keeps the system well above its ground state, even at zero temperature. A physically interesting feature of the steady state for rational ε is that grain orientations are *fully anticorrelated*. This is reminiscent of similar anticorrelations in grain displacements, associated with the collapse of bridges [14] in strongly compacted granular media. Also, while the macroscopic entropy of the steady state [16] is approximately that of a fully disordered column, consistent with Edwards' 'flatness' hypothesis [1], an investigation of the occupation probabilities of single configurations reveals a lot of structure at this microscopic level. Lastly, the low-temperature dynamics for irrational ε is characterised in terms of preferred nucleation sites, similar to the phenomenon of hierarchical melting observed in incommensurate modulated solids [19]. These sites 'nucleate' disorder, in the sense that, for a given irrational, they lead to the appearance of steady states corresponding to large rational approximants. It is tempting to compare these rational steady states (obtained as a result of low-temperature dynamics for *both* rational or irrational ε) with fluctuations around the so-called random close packing density [6, 22], which is the highest density achievable in practice by extensive dynamical processes.

Acknowledgements

AM warmly acknowledges the hospitality of the Service de Physique Théorique, Saclay, within whose tranquil surroundings most of this work was conceived.

A Distribution of the depth $\mathcal{N}$ of the upper layer

This Appendix is devoted to the depth $\mathcal{N}(t)$ of the ordered layer for low-temperature dynamics in the irrational case. Our main goal is to derive the stationary distribution of $\mathcal{N}$, for the effective dynamics described in section 5.1.

For convenience we use a continuous formalism, treating $\mathcal{N}$ as a real variable. Let $\pi(x)\,\mathrm{d}x$ be the nucleation rate per unit time between x and $x+\mathrm{d}x$, and $p(x,t)\,\mathrm{d}x$ be the probability of finding the depth $\mathcal{N}$ between x and $x+\mathrm{d}x$ at time t. The probability distribution function $p(x,t)$ obeys the rate equation

$$\left(\frac{\partial}{\partial t}+V\frac{\partial}{\partial x}\right)p(x,t)=\pi(x)P(x,t)-p(x,t)\Pi(x)\equiv\frac{\partial}{\partial x}\Big(\Pi(x)P(x,t)\Big), \tag{A.1}$$

with the notations

$$P(x,t)=\int_x^\infty p(y,t)\,\mathrm{d}y,\quad p(x,t)=-\frac{\partial P(x,t)}{\partial x},\qquad \Pi(x)=\int_0^x\pi(y)\,\mathrm{d}y,\quad \pi(x)=\frac{\mathrm{d}\Pi(x)}{\mathrm{d}x}. \tag{A.2}$$

Indeed, the left-hand side of (A.1) is the usual covariant derivative, whose convective term involves the drift velocity V. The middle side represents the evolution due to nucleation events, with the first (gain) term originating in nucleation at depth x, and the second (loss) term originating in nucleation at depth $y<x$.

The stationary (time-independent) solution $p_{\mathrm{stat}}(x)$ of (A.1) is such that

$$V\,p_{\mathrm{stat}}(x)\equiv -V\frac{\mathrm{d}P_{\mathrm{stat}}(x)}{\mathrm{d}x}=\Pi(x)P_{\mathrm{stat}}(x). \tag{A.3}$$

This separable differential equation easily yields the results

$$P_{\mathrm{stat}}(x)=\exp\left(-\frac{1}{V}\int_0^x\Pi(y)\,\mathrm{d}y\right),\qquad p_{\mathrm{stat}}(x)=\frac{\Pi(x)}{V}\exp\left(-\frac{1}{V}\int_0^x\Pi(y)\,\mathrm{d}y\right), \tag{A.4}$$

and especially

$$\begin{aligned}\langle\mathcal{N}\rangle&=\int_0^\infty\exp\left(-\frac{1}{V}\int_0^x\Pi(y)\,\mathrm{d}y\right)\mathrm{d}x\\&=\int_0^\infty\exp\left(-\frac{1}{V}\int_0^x(x-y)\pi(y)\,\mathrm{d}y\right)\mathrm{d}x.\end{aligned} \tag{A.5}$$

These expressions hold for an arbitrary distribution of nucleation rates.

In the case of interest in section 5.1, taking into account the leading sequence of Fibonacci sites F_k, with nucleation rates Π_k, we obtain

$$\langle\mathcal{N}\rangle=\sum_{k=0}^\infty\frac{V}{A_k}\left(\mathrm{e}^{-B_k/V}-\mathrm{e}^{-B_{k+1}/V}\right), \tag{A.6}$$

with

$$A_k=\sum_{\ell=0}^{k}\Pi_\ell,\qquad B_k=\sum_{\ell=0}^{k-1}(F_k-F_\ell)\Pi_\ell. \tag{A.7}$$

References

[1] S.F. Edwards, in *Granular Matter: An Interdisciplinary Approach*, ed. A. Mehta (Springer, New York, 1994).

[2] P.G. de Gennes, Rev. Mod. Phys. **71**, S374 (1999).

[3] M.F. Shlesinger and J.T. Bendler, in *Phase Transitions in Soft Condensed Matter*, T. Riste and D. Sherrington, eds. (Plenum, 1989); R. Monasson, Phys. Rev. Lett. **75**, 2847 (1995); E. Marinari, G. Parisi, F. Ricci-Tersenghi, and F. Zuliani, J. Phys. A **34**, 383 (2001); L. Berthier, L.F. Cugliandolo, and J.L. Iguain, Phys. Rev. E **63**, 051302 (2001); M. Mézard, Physica A **306**, 25 (2002); G. Biroli and M. Mézard, Phys. Rev. Lett. **88**, 025501 (2002); A. Lawlor, D. Reagan, G.D. McCullagh, P. De Gregorio, P. Tartaglia, and K.A. Dawson, Phys. Rev. Lett. **89**, 245503 (2002).

[4] P.F. Stadler, A. Mehta, and J.M. Luck, Adv. Complex Systems **4**, 429 (2001).

[5] A. Mehta and J.M. Luck, J. Phys. A **36** (2003), in press (cond-mat/0211286).

[6] R.L. Brown and J.C. Richards, *Principles of Powder Mechanics* (Pergamon, Oxford, 1970).

[7] M. Mézard, G. Parisi, and M.A. Virasoro, *Spin Glass Theory and Beyond* (World Scientific, Singapore, 1987).

[8] P.F. Stadler, J.M. Luck, and A. Mehta, Europhys. Lett. **57**, 46 (2002).

[9] N.G. de Bruijn, Nederl. Akad. Wetens. Proc. A **84**, 27 (1981); M. Duneau and A. Katz, Phys. Rev. Lett. **54**, 2688 (1985); J. Phys. (France) **47**, 181 (1986); V. Elser, Phys. Rev. B **32**, 4892 (1985); P.A. Kalugin, A.Yu. Kitayev, and L.S. Levitov, JETP Lett. **41**, 145 (1985); J. Phys. (France) Lett. **46**, L601 (1985).

[10] G.H. Hardy and E.M. Wright, *An Introduction to the Theory of Numbers* (Clarendon, Oxford, 1990).

[11] A.J. Bray, Adv. Phys. **43**, 357 (1994).

[12] E.R. Nowak, J.B. Knight, M. Povinelli, H.M. Jaeger, and S.R. Nagel, Powder Technology **94**, 79 (1997); E.R. Nowak, J.B. Knight, E. Ben-Naim, H.M. Jaeger, and S.R. Nagel, Phys. Rev. E **57**, 1971 (1998); E.R. Nowak, A. Grushin, A.C.B. Barnum, and M.B. Weissman, Phys. Rev. E **63**, 020301 (2001).

[13] S.J. Cornell, K. Kaski, and R.B. Stinchcombe, Phys. Rev. B **44**, 12263 (1991); S.J. Cornell and A.J. Bray, Phys. Rev. E **54**, 1153 (1996); V. Spirin, P.L. Krapivsky, and S. Redner, Phys. Rev. E **60**, 2670 (1999).

[14] A. Mehta and G.C. Barker, Phys. Rev. Lett. **67**, 394 (1991); G.C. Barker and A. Mehta, Phys. Rev. A **45**, 3435 (1992); Phys. Rev. E **47**, 184 (1993); A. Mehta and G.C. Barker, Europhys. Lett. **27**, 501 (1994); J. Phys. Cond. Matt. **12**, 6619 (2000).

[15] E.R. Weeks and D.A. Weitz, Chem. Phys. **284**, 361 (2002).

[16] R. Monasson and O. Pouliquen, Physica A **236**, 395 (1997).

[17] S.F. Edwards and D.V. Grinev, Phys. Rev. E **58**, 4758 (1999).

[18] J.M. Luck, C. Godrèche, A. Janner, and T. Janssen, J. Phys. A **26**, 1951 (1993); J.M. Luck, in *Fundamental Problems in Statistical Mechanics VIII*, eds. H. van Beijeren and M.H. Ernst (Elsevier, Amsterdam, 1994).

[19] F. Vallet, R. Schilling, and S. Aubry, Europhys. Lett. **2**, 815 (1986); R. Schilling and S. Aubry, J. Phys. C **20**, 4881 (1987); F. Vallet, R. Schilling, and S. Aubry, J. Phys. C **21**, 67 (1988).

[20] J. Berg and A. Mehta, Europhys. Lett. **56**, 784 (2001); Phys. Rev. E **65**, 031305 (2002).

[21] S. Torquato, *Random Heterogeneous Materials: Microstructure and Macroscopic Properties* (Springer, New York, 2001).

[22] J.D. Bernal, Proc. R. Soc. London A **280**, 299 (1964).